RSC Advances

PAPER

View Article Online
View Journal | View Issue

Cite this: *RSC Adv.*, 2014, **4**, 33549

Electronic transitions and dielectric function tensor of a $YMnO_3$ single crystal in the NIR-VUV spectral range

Rüdiger Schmidt-Grund,*[a] Steffen Richter,[a] Stefan G. Ebbinghaus,[b] Michael Lorenz,[a] Carsten Bundesmann[c] and Marius Grundmann[a]

Received 28th May 2014
Accepted 23rd July 2014

DOI: 10.1039/c4ra05036c

www.rsc.org/advances

We present optical properties in the near-infrared to vacuum-ultraviolet spectral range of hexagonal $YMnO_3$. The high-quality (110)-oriented bulk single crystal was grown by the optical floating zone technique. We have determined the tensor of the dielectric function by means of Mueller matrix ellipsometry in the wide spectral range (0.5–9.15) eV. For the spectral range below 5.4 eV, we present much more precise data compared to previous reports. For higher energies no experimental reports were given previously. The experimental dielectric function of $YMnO_3$ agrees generally with theoretical calculations. We found the well known transitions involving hybridized oxygen – Mn states and Mn-3d states to be spectrally localized with a homogeneous Lorentzian lineshape. At energies above these transitions, we observe pseudo-transparent points where for each of the principal diagonal elements of the dielectric function tensor the imaginary part approaches zero but at different photon energies. These are followed at the onset of the high-absorption spectral range by parabolic direct band–band transitions which have not been reported so far.

1 Introduction

Rare earth ("R") manganites $RMnO_3$ (RMO) are in the focus of research since the last ten years because of their interesting ferroelectric, magnetic or even multiferroic properties at low temperatures (*cf.* the reviews 1–6 and references therein). Among these manganites, hexagonal $YMnO_3$ (YMO) is a special case because of its strong magneto-electric interaction, caused by the interplay between Mn ions and O ions in a distorted close-packed configuration.[1,7] A connection between this property and a characteristic interband charge transfer transition from the hybridized oxygen – Mn states to Mn-3d states in the dielectric function spectra at ≈1.6 eV is proposed.[8] This transition is also found for some other hexagonal RMO. Magnetic field dependence of the optical absorption and second order susceptibility indicates for some of them coupling of electronic charge distribution and magnetic ordering at low temperature.[9,10] The optical properties[11] of YMO at photon energies up to ≈5 eV have been experimentally and theoretically widely studied.[8–10,12–14] Its dielectric function tensor has been theoretically derived for energies up to 15 eV,[12] but experimental data are only available for the spectral range (0.7–5.4) eV.[13] In the latter publication, the dielectric function tensor has been investigated by means of spectroscopic ellipsometry, but without Kramers–Kronig consistent modelling of the data. Thus, surface effects and sample alignment artefacts are possibly included in that data. For understanding the electronic structure of YMO, a precise knowledge of the properties of electronic transitions and their symmetry in a wide spectral range is very important, which can be derived *e.g.* from the material's dielectric function tensor.

In the following we first describe shortly growth and structural properties of the sample, the experimental determination of the Mueller matrix and the model analysis procedure applied for determination of the dielectric function tensor in the NIR-VUV spectral range. Finally, we discuss the features observed in the dielectric function tensor and compare them with theoretical predictions.

2 Experimental details

2.1 Growth and structure properties

The bulk YMO sample was grown by the optical floating zone technique. Stoichiometric amounts (0.025 mol) of pre-dried Y_2O_3 and Mn_2O_3 were thoroughly ground using agate mortar and pestle. The mixture was calcined in air at 1000 °C for 12 h and 1200 °C for 24 h with intermediate re-grinding. Rods of the

[a]*Fakultät für Physik und Geowissenschaften, Institut für Experimentelle Physik II, Universität Leipzig, Linnéstr. 5, D-04103 Leipzig, Germany. E-mail: Schmidt-Grund@physik.uni-leipzig.de; Fax: +49 0341 9732668; Tel: +49 0341 9732619*

[b]*Institut für Chemie, Martin-Luther-Universität Halle-Wittenberg, Kurt-Mothes-Straße 2, D-06120 Halle/Saale, Germany*

[c]*Leibniz-Institut für Oberflächenmodifizierung (IOM), Permoserstr. 15, D-04318 Leipzig, Germany*

polycrystalline material were sintered in air at 1600 °C for 24 h on a platinum coated boat. Crystal growth in synthetic air (flow rate 100 ml min^{-1}) was carried out using a CSC optical floating zone furnace model FZ-T-10000-H-VPO-PC equipped with four 1500 W halogen lamps. The feed and seed rods were counter-rotated with 30 rpm. The resulting crystal of about 5 mm diameter and 50 mm length was cut perpendicular to the growth direction. The surfaces of the crystal slices (≈1 mm thick) were polished with 1 μm diamond suspension. Therefore, the surface exhibits some scratches, but the flat surface in between shows a roughness of about $R_{rms} \approx 1$ nm as determined by atomic force microscopy.

The crystal structure was investigated by means of single crystal X-ray diffraction (XRD) using a STOE IPDS-2T diffractometer operating with Mo–K radiation. A very good structure refinement ($R_1 = 0.0176$, w$R_2 = 0.0398$) was achieved, indicating a high crystal quality. Details of the crystal structure investigations may be obtained from the Fachinformationszentrum Karlsruhe, D-76344 Eggenstein-Leopoldshafen (Germany), on quoting the depository number CSD-427158. The results are in accordance with earlier single crystal X-ray investigations.[15–19] Our crystals were found to be racemic (inversion) twins with 50% contribution of both domains within experimental uncertainties as already described for other samples.[17,19]

The orientation and mosaicity of the YMO single crystal was determined by high-resolution X-ray diffraction (HR-XRD) using a PANalytical X'pert PRO MRD diffractometer with incident Cu Kα parallel beam. The rocking curve of the (110) reflection of the YMO single crystal was measured with X-ray mirror with 1/32° divergence slit, 4× Ge(220) monochromator and (1.5 × 1.5) mm^2 cross slit, *i.e.* Cu $K\alpha_1$ radiation with 12 arcsec primary divergence. The detector was a PIXcel^{3D} array operated in 1D scanning mode ($2\theta - \omega$ scans) or in 0D open mode (rocking curves), respectively. (110) orientation (so-called *a*-plane) with ≈10° cut-off was found and the full-width-at-half-maximum (FWHM) of the (110) omega scan (rocking curve) is 100 arcsec which indicates a low mosaicity of the YMO sample (Fig. 1).

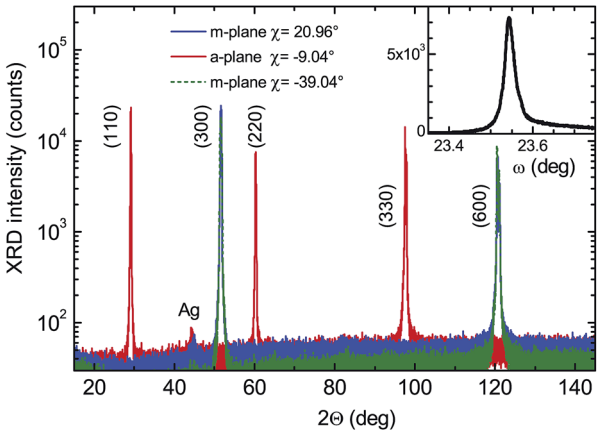

Fig. 1 XRD $2\theta - \omega$ scans and rocking curve of the (110) reflex: $2\theta - \omega$ scans of a first *m*-plane (blue line), the *a*-plane (red line), and the next *m*-plane (green line) of the hexagonal structure, measured by rotating the YMO single crystal around its in-plane *c*-axis by three values for χ as labelled. There is no simple lattice plane parallel to the sample surface. The weak Ag signal stems from silver paste used to fix the crystal for temperature dependent measurements. The inset shows the HR-XRD rocking curve of the (110) reflex at $\chi = -9.04°$. The FWHM is 100 arcsec.

2.2 Spectroscopic ellipsometry

The dielectric function tensor was determined by means of Mueller matrix spectroscopic ellipsometry[20] in a wide spectral range from 0.5 eV to 9.15 eV at room temperature using two commercial spectroscopic ellipsometers, namely of dual rotating compensator type for measuring the full 4 × 4 Mueller matrix for photon energies (0.75–6.4) eV and of rotating analyser type equipped with one compensator in the whole spectral range (by the latter, only the first three rows of the Mueller matrix are measured). Measurements were performed at 16 different in-plane orientations ϕ[21] of the crystal *c*-axis, which coincides with the optical axis, with respect to the plane of incidence in the full range $\phi = (0–360)°$, covering also the special cases parallel ($\phi = 0°$, 180°) and perpendicular ($\phi = 90°$, 270°) at which no energy conversion between the *p*- and *s*-polarized eigenmodes of the probe beam[22] takes place,[20] and in a wide range of angles of incidence between $\Phi = 45°$ and 75° with respect to the sample surface normal. The Φ–ϕ-evolution of the Mueller matrix spectra clearly reveals optical uniaxiality with the optical axis within the sample's surface plane ($\theta = (91.9 \pm 1)°$ (ref. 21)). The symmetry of the full Mueller matrix (Fig. 2) proofs optical reciprocity as expected because for the room temperature paramagnetic phase of YMO[23] no magneto-optical effects should occur.

The experimental data were analysed using a transfer-matrix technique considering a three-phase model consisting of the half-infinite YMO single crystal and a thin surface layer, found to be effectively ≈6 nm thick, bounded by the ambient. The surface was assumed to show some roughness without any chemical modification, thus a standard Bruggeman-type effective-medium approximation[24] was applied by mixing the dielectric functions of YMO (≈65%) and void (≈35%), and with a depolarization factor of about one, in order to account for the mentioned scratches. These scratches do not significantly influence the ellipsometric measurements because they basically cause scattering of light which then is not collected by the detector. A weak depolarization in the experimental Mueller matrix spectra is caused which was modelled assuming a patterned surface layer (≈1/4 is not covered). For a hexagonal crystal structure, the complex dielectric function tensor in the principle axis representation has only elements $\tilde{\varepsilon}_{ij}$ different from zero at the main diagonal, where $\tilde{\varepsilon}_{\perp} = \tilde{\varepsilon}_{11} = \tilde{\varepsilon}_{22} \neq \tilde{\varepsilon}_{33} = \tilde{\varepsilon}_{\parallel}$.[20] The complex dielectric functions $\tilde{\varepsilon}_{\perp,\parallel} = \varepsilon_{1;\perp,\parallel} + i\varepsilon_{2;\perp,\parallel}$ of YMO were determined by Kramers–Kronig-consistent mathematical inversion[25] simultaneously invoking the whole experimental data set using a regression analysis with a Levenberg–Marquardt algorithm. The model calculated Mueller matrix elements are included in the Fig. 2a–c.

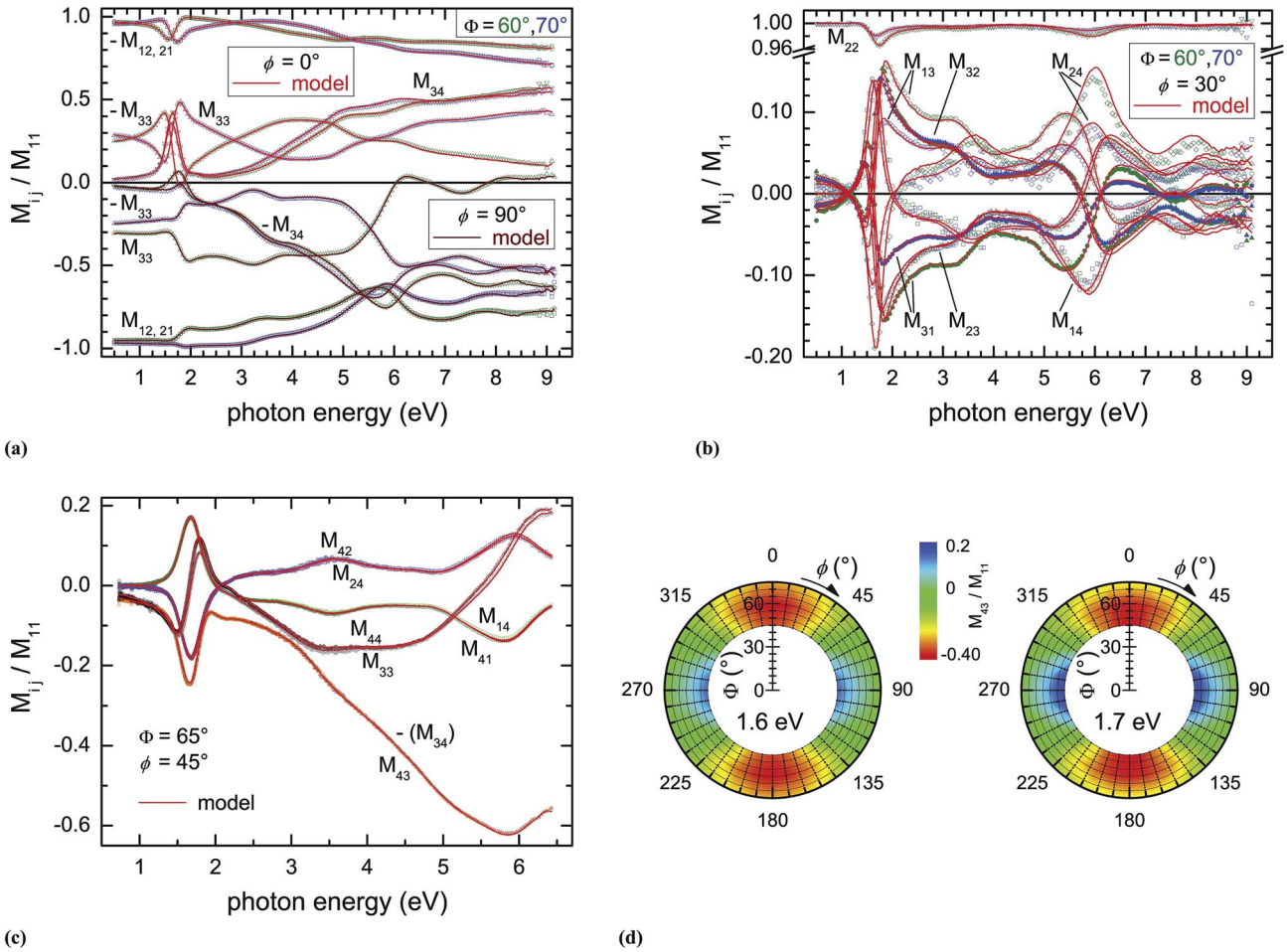

Fig. 2 Experimental (symbols) and model calculated (lines) spectra of the Mueller matrix elements. (a and b) In the entire spectral range (first three rows of the Mueller matrix): (a) diagonal elements for in-plane orientation $\phi = 0°$ (upper part) and 90° (lower part), the off-diagonal elements are zero and $M_{22} = 1$; (b) off-diagonal elements and M_{22} for in-plane orientation $\phi = 30°$. (c) Mueller matrix elements which are sensitive to optical non-reciprocity and circular birefringence for in-plane orientation $\phi = 45°$. It is found $M_{43} = -M_{34}$ with a standard deviation of ≈0.002 which is within the accuracy of the Mueller matrix elements, the other pairs M_{i4}/M_{4i} and M_{33}/M_{44} differ slightly from each other due to the linear birefringence which is nicely reproduced by the model. (d) Colour coded images of the $\Phi - \phi$-evolution of the experimental M_{43} at photon energies 1.6 eV and 1.7 eV. (a–d) The uncertainty in the experimental Mueller matrix elements is below 0.003 for photon energies <6.5 eV and increases to ≈0.01 for 9.15 eV.

3 Results and discussion

The spectra of the elements $\varepsilon_{1;\perp,\parallel}$ and $\varepsilon_{2;\perp,\parallel}$ of the complex dielectric function tensor are shown in Fig. 3a and the spectra of the derived absorption coefficients in Fig. 4a. Spectra of the linear birefringence $\Delta n = n_\perp - n_\parallel$ and linear dichroism $\Delta\kappa = \kappa_\perp - \kappa_\parallel$ are shown in Fig. 4b. In the NIR-UV spectral range features of electronic transitions observed previously in YMO[13,14] and related hexagonal manganites[3,8–10] are basically reflected. At energies above 5 eV, two more pronounced features occur in the dielectric function spectra presented here. Also theoretically predicted transitions shown in ref. 12 are basically reflected in the entire spectral range. Fig. 3b shows a comparison of both, the experimental and theoretical (ref. 12) data set for ε_2.

In the following we will discuss properties of the dielectric function spectra which have been observed for the first time in the data presented here with regard to knowledge from literature. Table 1 summarizes parameters of the most important observations.

(I) The pronounced absorption feature due to interband charge transfer transitions from the hybridized oxygen – Mn states to Mn-3d states[8] at the onset of the absorption has been observed in the literature experimentally and was predicted theoretically.[8,9,12–14] Its energetic position was found in the here presented data at 1.612 eV ($\varepsilon_{2;\perp}$) and 1.686 eV ($\varepsilon_{2;\parallel}$), roughly in the range of other experimental observations. It should be noted that the anisotropic properties of this transition has been reported experimentally in ref. 13 only. In the theoretical dielectric function spectra, it is predicted for $\varepsilon_{2;\perp}$ at ≈0.65 eV but does not appear in $\varepsilon_{2;\parallel}$ at all (*cf.* also VII and the note 27).[12] Differently to previous observations and also to the theoretical prediction, we found that these transitions are spectrally discrete, *i.e.* they are each followed at higher energies by a

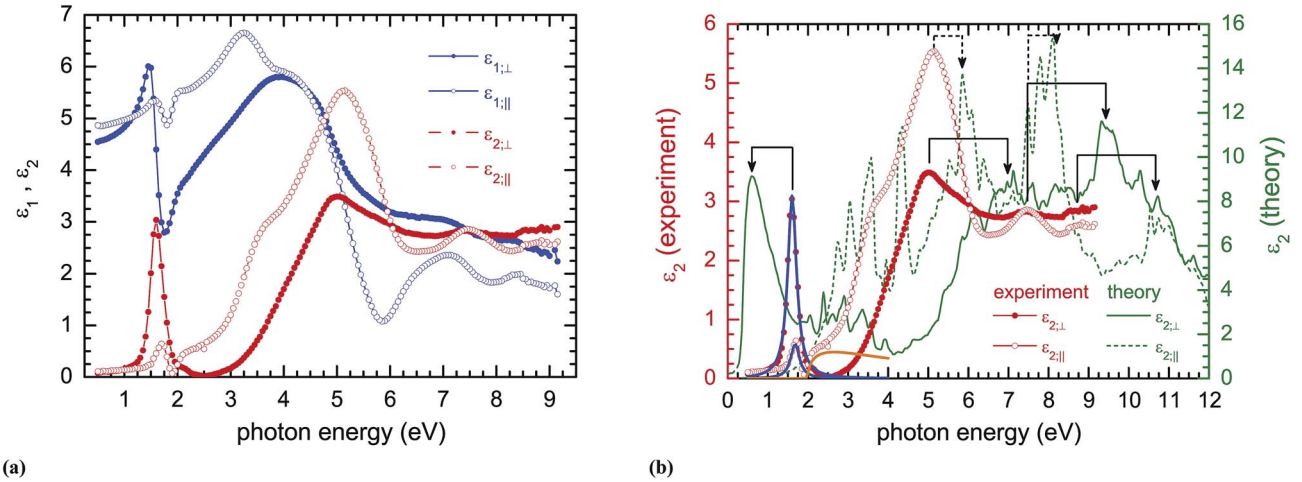

Fig. 3 (a) Spectra of the dielectric function tensor elements $\varepsilon_{1;\perp,\parallel}$ (blue symbols, $\perp$: filled, $\parallel$: open) and $\varepsilon_{2;\perp,\parallel}$ (red symbols, $\perp$: filled, $\parallel$: open). Lines are guides for the eye, only (please note comment 26 regarding the data uncertainty). (b) Comparison of the experimental $\varepsilon_{2;\perp,\parallel}$ spectra (red symbols, $\perp$: filled, $\parallel$: open) with theoretical calculated ones reproduced from ref. 12 (green lines, $\perp$: solid, $\parallel$: dashed). The arrows indicate the assignment of the peaks observed in experiment to that in theory (solid lines: $\varepsilon_{2;\perp}$, dashed lines: $\varepsilon_{2;\parallel}$). Please note the different scale of the ε_2-axes for experiment (left) and theory (right). The blue lines show Lorentzian lineshape approximations of the sharp peaks at 1.612 eV ($\varepsilon_{2;\perp}$) and 1.686 eV ($\varepsilon_{2;\parallel}$). The orange line represents the M0 critical point-like onset of the band-band absorption of $\varepsilon_{2;\parallel}$ at 1.97 eV. Please note that here only the contribution of the M0 transition is plotted. If neighboured transitions are also considered, the model matches precisely the experimental data.

vanishing absorption or rather ε_2 (*cf.* (II)). Also we have found that their lineshape is Lorentzian and their broadening is purely homogeneous with the same value for both of $\approx$0.26 eV. This is demonstrated by the match of Lorentzians model functions to their lineshape (blue lines in Fig. 3b). Thus disorder effects on the lineshape can be excluded and the involved electronic states should be well defined with molecule-like characteristics. Regarding excitonic polarizabilities to be the nature of these transitions please see also (IV).

(II) We observe quasi-transparent points (*i.e.* $\varepsilon_2 \rightarrow 0$) in $\varepsilon_{2;\perp}$ at $\approx$2.5 eV and in $\varepsilon_{2;\parallel}$ at $\approx$1.9 eV, which is in both cases at the high energy side of the transitions discussed in (I) (please note the comment 26 regarding the data uncertainty). Such a behaviour was not observed previously.

(III) These quasi-transparent points are followed at higher energies by the onset of M0 critical point-like direct band-band absorption at 1.97 eV in $\varepsilon_{2;\parallel}$ (orange line in Fig. 3b) and, less pronounced, at $\approx$2.6 eV in $\varepsilon_{2;\perp}$ which was not observed experimentally before. In ref. 12, a direct band gap is theoretically proposed with 0.48 eV width at the Γ-point of the Brillouin zone and another with 2.5 eV between the M and K point. If one would consider the general difference in the energetic positions and the assignment of the structures observed in experiment to that in theory (VII and Fig. 3b) the band gap absorption predicted at 2.5 eV could be assigned to the M0-like transition found her in $\varepsilon_{2;\parallel}$ at $\approx$2 eV and possibly also to that at $\approx$2.6 eV in $\varepsilon_{2;\perp}$. In contrast, the band gap predicted at 0.48 eV cannot be assigned to one of the M0-like transitions observed here but it

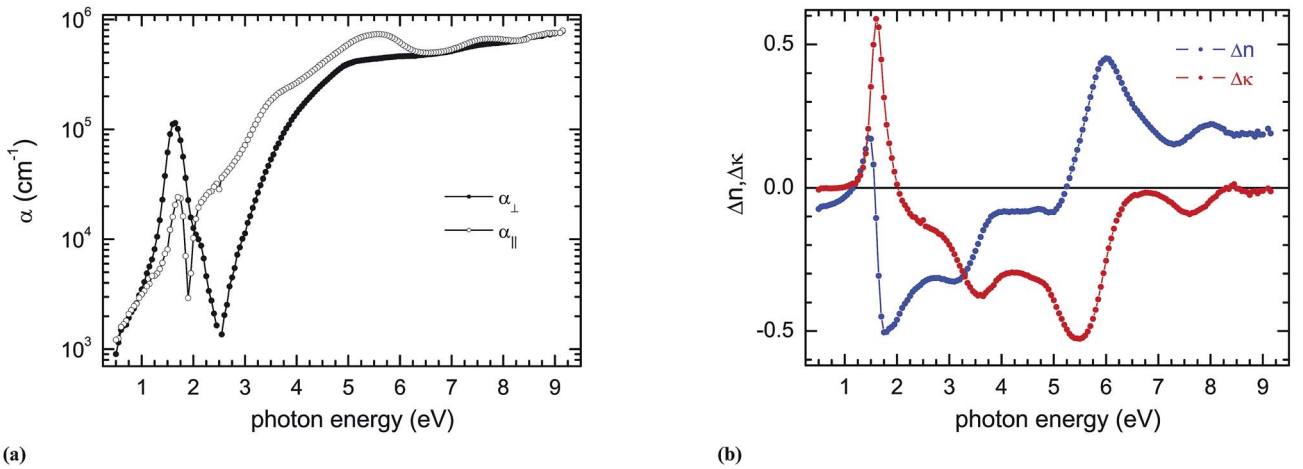

Fig. 4 Spectra of (a) the absorption coefficients $\alpha_{\perp,\parallel}$ (symbols, $\perp$: filled, $\parallel$: open) and (b) of the linear birefringence Δn (blue symbols) and dichroism $\Delta\kappa$ (red symbols). Lines are guides for the eye, only (please note comment 26 regarding the data uncertainty).

Table 1 Parameters of the most important features observed in the dielectric function spectra. The uncertainty is in the order of the last digit

		Energy (eV)		Broadening (eV)	Amplitude ratio
		$\varepsilon_{2;\perp}$	$\varepsilon_{2;\parallel}$	$\varepsilon_{2;\perp,\parallel}$	$A^{i}(\varepsilon_{2;\perp})/A^{i}(\varepsilon_{2;\parallel})$
(I)	Lorentzian absorption	1.612	1.686	0.26	5
(II)	Quasi-transparent points	2.5	1.90	—	—
(III)	M0-like band gap	2.6	1.97	0.02	1/5

rather fits, also in view of its lineshape in the dielectric function, to the transition discussed in (I).

(IV) The amplitude ratios for the Lorentzian (I) and M0-like (III) transitions between $\perp$ and $\parallel$ are found to behave inversely like $A^{\mathrm{Lorentz}}(\varepsilon_{2;\perp})/A^{\mathrm{Lorentz}}(\varepsilon_{2;\parallel}) \approx A^{\mathrm{M0}}(\varepsilon_{2;\parallel})/A^{\mathrm{M0}}(\varepsilon_{2;\perp}) \approx 5$.[27] This indicates some correlation between both types of transitions. Solely excitonic effects can be excluded because, apart from the fact that these Lorentzian transitions are well-known and assigned to the above mentioned transitions in literature,[8,9,13,14] amplitudes of excitonic polarizabilities and the band–band transitions they are related to should be proportional to each other *via* the transfer matrix elements.

As some general remarks regarding the shape of the dielectric function spectra we want to point out:

(V) In comparison to the dielectric function shown in ref. 13, the data presented here are Kramers–Kronig consistent, by far less noisy and also the absolute values and the lineshape differ considerably. This is especially the case for the real part, where for $\varepsilon_{1;\parallel}$ features present in the imaginary part are not reflected, probably caused by lack of Kramers–Kronig consistency of the data shown in ref. 13. Thus, the data presented here provide a more reliable basis for electronic structure calculations.

(VI) The Lorentzian transitions (I) and the strong transitions observed in ε_2 at $\approx$(3–6) eV show a pronounced dichroism (*cf.* Fig. 4b). In the VUV spectral range the spectral weight is almost equally distributed within the directions $\perp$ and $\parallel$. The small linear birefringence at high energies suggests that electronic transitions at energies above the spectral range investigated here are more pronounced for $\varepsilon_{\perp}$. Further, the relatively small absolute values of ε_1 which are only twice that of the vacuum dielectric constant ($\varepsilon_{1,\infty} = 1$, $\varepsilon = \varepsilon_0$) and its smooth lineshape in this spectral range further suggest that the overall spectral weight of those transitions can be assumed to be not very high, which confirms theoretical predictions for YMO[12,28,29] and is similar to other manganites.[3,30]

(VII) The transitions observed in the dielectric function spectra presented here compared to the theoretically predicted (ref. 12) are energetically shifted against each other and differently spectrally broadened (Fig. 3b).[31] Also, more features are predicted in the theoretical dielectric functions. Regarding the spectral broadening, based on the homogeneous lineshape found for the Lorentzian transitions (*c.f.* (I)), all experimentally observed transitions are assumed to be homogeneously broadened and to be not affected by disorder effects. Thus it can be concluded that theory overestimates the number of different electronic transitions, even if lifetime effects would be included in the theoretical spectra. Temperature effects induced by electron–phonon interaction to be responsible for the large broadening observed in the experimental spectra and the different energies of the observed and theoretically predicted transitions can be assumed to be negligible.[31] Besides general limitations of first principle calculations, the energy shift found between the experimental and theoretical dielectric function spectra (Fig. 3b) could, at least partially, be related to neglecting excitonic effects in the theory.[12,32,33] Thus, comparing the general lineshape, one can choose the assignment of transitions observed in the experimental dielectric function to those predicted theoretically as indicated by the arrows in Fig. 3b.

4 Conclusions

We have determined Kramers–Kronig consistently the dielectric function tensor of a hexagonal $YMnO_3$ bulk single crystal with high precision by means of Mueller matrix spectroscopic ellipsometry in the wide spectral range (0.5–9.15) eV at room temperature. The symmetry of the 4 × 4 Mueller matrices proves the optical linear uniaxial behaviour. The experimental dielectric function tensor compares generally well to a theoretically predicted one. For the first time, we have observed a M0 critical point-like band-band transition in each of the tensor components $\tilde{\varepsilon}_{\perp}$ and $\tilde{\varepsilon}_{\parallel}$ and pseudo-transparent points between them and the pronounced discrete transitions involving Mn-3d states which we have found to be purely Lorentzian with a homogeneous broadening.

Acknowledgements

We acknowledge L. Fricke for AFM measurements as well as H. Franke and C. Sturm for reading the manuscript and valuable discussions. This work was supported by Deutsche Forschungsgemeinschaft (DFG) within Sonderforschungsbereich 762 – "Functionality of Oxide Interfaces"(INST271/240-2, A8 and B3). The optical floating zone furnace was supported by the DFG through grant INST 271/258-1 FUGG.

Notes and references

1 J. P. Velev, S. S. Jaswal and E. Y. Tsymbal, *Philos. Trans. R. Soc., A*, 2011, **369**, 3069.
2 G. Lawes and G. Srinivasan, *J. Phys. D: Appl. Phys.*, 2011, **44**, 243001.

3 A. S. Moskvin and R. V. Pisarev, *Low Temp. Phys.*, 2010, **36**, 489.
4 S. Dong and J.-M. Liu, *Mod. Phys. Lett. B*, 2012, **26**, 1230004.
5 A. M. Shuvaev, A. A. Mukhin and A. Pimenov, *J. Phys.: Condens. Matter*, 2011, **23**, 113201.
6 B. Lorenz, *Condens. Matter Phys.*, 2013, **2013**, 497073.
7 B. B. van Aken, T. T. M. Palstra, A. Filipetti and N. A. Spaldin, *Nat. Mater.*, 2004, **3**, 164.
8 W. S. Choi, D. G. Kim, S. S. A. Seo, S. J. Moon, D. Lee, J. H. Lee, H. S. Lee, D.-Y. Cho, Y. S. Lee, P. Murugavel, J. Yu and T. W. Noh, *Phys. Rev. B*, 2008, **77**, 045137.
9 W. S. Choi, S. J. Moon, S. S. A. Seo, D. Lee, J. H. Lee, P. Murugavel, T. W. Noh and Y. S. Lee, *Phys. Rev. B*, 2008, **78**, 054440.
10 R. C. Rai, J. Cao, J. L. Musfeldt, S. B. Kim, S. W. Cheong and X. Wei, *Phys. Rev. B*, 2007, **75**, 184414.
11 We restrict the discussion here only to the near-infrared to vacuum-ultraviolet spectral range.
12 M. Qian, J. Dong and D. Y. Xing, *Phys. Rev. B*, 2000, **63**, 155101.
13 A. M. Kalashnikova and R. V. Pisarev, *JETP Lett.*, 2003, **78**, 143.
14 W.-C. Yi, S.-I. Kwun and J.-G. Yoon, *J. Phys. Soc. Jpn.*, 2000, **69**, 2706.
15 U. Salazar-Kuri, M. E. Mendoza and J. M. Siqueiros, *Phys. B*, 2012, **407**, 3551.
16 S. Lee, A. Pirogov, M. Kang, K.-H. Jang, M. Yonemura, T. Kamiyama, S.-W. Cheong, F. Gozzo, N. Shin, H. Kimura, Y. Noda and J.-G. Park, *Nature*, 2008, **451**, 805.
17 G. Nénert, M. Pollet, S. Marinel, G. R. Blake, A. Meetsma and T. T. M. Palstra, *J. Phys.: Condens. Matter*, 2007, **19**, 466212.
18 T. Katsufuji, M. Masaki, A. Machida, M. Moritomo, K. Kato, E. Nishibori, M. Takata, M. Sakata, K. Ohoyama, K. Kitazawa and H. Takagi, *Phys. Rev. B*, 2002, **66**, 134434.
19 B. van Aken, *Acta Crystallogr., Sect. C: Cryst. Struct. Commun.*, 2001, **57**, 230.
20 H. Fujiwara, *Spectroscopic ellipsometry: principles and applications*, John Wiley and Sons, 2007.
21 θ and ϕ are two out of the three Euler angles describing the tilt with respect to the surface normal and the in-plane orientation with respect to the propagation direction of the probe beam of the optical axis, respectively.[20]
22 *p* and *s* refers to the linear polarization parallel and perpendicular to the plane of incidence, respectively, which is spanned by the propagation direction of the probe beam and the surface normal of the sample.[20]
23 R. I. Thomson, T. Chatterji, C. J. Howard, T. T. M. Palstra and M. A. Carpenter, *J. Phys.: Condens. Matter*, 2014, **26**, 045901.
24 J. Jellison, L. A. Boatner, D. H. Lowndes, R. A. McKee and M. Godbole, *Appl. Opt.*, 1994, **33**, 6053.
25 The high energy extrapolation for the Kramers–Kronig analysis was done using an pole function, *i.e.* a undamped harmonic oscillator.
26 The absolute values of the dielectric function tensor elements are hard to determine with great precision because they are strongly correlated with the exact treatment of the surface layer and the exact value of θ. Thus $\varepsilon_2 \rightarrow 0$ is not exactly determined. An average uncertainty for all $\delta\varepsilon$ of approximately $+0.2/-0.05$ can be estimated. In the VUV spectral range $\delta\varepsilon$ is somewhat smaller but larger in the range 1–5 eV (up to $+0.5/-0.05$). It should be noted that $\delta\varepsilon$ is almost isotropic, that means the linear birefringence and dichroism are not affected too much.
27 Please note that in our data the appearance of the Lorentzian peak in the $\varepsilon_{\|}$ tensor element cannot be caused in a sample misalignment during the ellipsometry experiments. Based on the large experimental data set, the sample orientation and Euler angles are determined very precisely and thus also the contribution to each of the dielectric function tensor elements are well defined in energy and amplitude and separated well from each other.[26]
28 J. E. Medvedeva, V. I. Anisimov, M. A. Korotin, O. N. Mryasov and A. J. Freeman, *J. Phys.: Condens. Matter*, 2000, **12**, 4947.
29 C. Zhong, Q. Jiang, H. Zhang and X. Jiang, *Appl. Phys. Lett.*, 2009, **94**, 224107.
30 A. Rusydi, R. Rauer, G. Neuber, M. Bastjan, I. Mahns, S. Müller, P. Saichu, B. Schulz, S. G. Singer, A. I. Lichtenstein, D. Qi, X. Gao, X. Yu, A. T. S. Wee, G. Stryganyuk, K. Dörr, G. A. Sawatzky, S. L. Cooper and M. Rübhausen, *Phys. Rev. B*, 2008, **78**, 125110.
31 It shall be mentioned that the calculations in ref. 12 have been done for zero Kelvin and for the antiferromagnetic ordered phase. First results regarding low temperature dielectric function spectra indicate a basically similar lineshape as the room temperature data presented here. This is especially true for the linewidth, thus it can be assumed that the interaction of the electronic system with phonons does not dominantly contribute to the observed broadening.
32 T. Iizuka-Sakano, E. Hanamura and Y. Tanabe, *J. Phys.: Condens. Matter*, 2001, **13**, 3031.
33 C. Degenhardt, M. Fiebig, D. Fröhlich, Th. Lottermoser and R. V. Pisarev, *Appl. Phys. B*, 2001, **73**, 139.

